microPET and Autoradiographic Imaging of GRP Receptor Expression with ^{64}Cu-DOTA-[Lys^3]Bombesin in Human Prostate Adenocarcinoma Xenografts

Xiaoyuan Chen, PhD; Ryan Park, BS; Yingping Hou, MD; Michel Tohme, MS; Antranik H. Shahinian, BS; James R. Bading, PhD; and Peter S. Conti, MD, PhD

PET Imaging Science Center, University of Southern California Keck School of Medicine, Los Angeles, California

Overexpression of gastrin-releasing peptide (GRP) receptor (GRPR) in both androgen-dependent (AD) and androgen-independent (AI) human neoplastic prostate tissues provides an attractive target for prostate cancer imaging and therapy. The goal of this study was to develop ^{64}Cu-radiolabeled GRP analogs for PET imaging of GRPR expression in prostate cancer xenografted mice. **Methods:** [Lys^3]bombesin ([Lys^3]BBN) was conjugated with 1,4,7,10-tetraazadodecane-*N,N′,N″,N‴*-tetraacetic acid (DOTA) and labeled with the positron-emitting isotope ^{64}Cu (half-life = 12.8 h, 19% β^+). Receptor binding of DOTA-[Lys^3]BBN and internalization of ^{64}Cu-DOTA-[Lys^3]BBN by PC-3 prostate cancer cells were measured. Tissue biodistribution, microPET, and whole-body autoradiographic imaging of the radiotracer were also investigated in PC-3 (AI)/CRW22 (AD) prostate cancer tumor models. **Results:** A competitive receptor- binding assay using ^{125}I-[Tyr^4]BBN against PC-3 cells yielded a 50% inhibitory concentration value of 2.2 ± 0.5 nmol/L for DOTA-[Lys^3]BBN. Incubation of cells with the ^{64}Cu-labeled radiotracer showed temperature- and time-dependent internalization. At 37°C, >60% of the tracer was internalized within the first 15 min and uptake remained constant for 2 h. Radiotracer uptake was higher in AI PC-3 tumor (5.62 ± 0.08 %ID/g at 30 min after injection, where %ID/g is the percentage of injected dose per gram) than in AD CWR22 tumor (1.75 ± 0.05 %ID/g at 30 min after injection). Significant accumulation of the activity in GRPR-positive pancreas was also observed (10.4 ± 0.15 %ID/g at 30 min after injection). Coinjection of a blocking dose of [Lys^3]BBN inhibited the activity accumulation in PC-3 tumor and pancreas but not in CWR22 tumor. microPET and autoradiographic imaging of ^{64}Cu-DOTA-[Lys^3]BBN in athymic nude mice bearing subcutaneous PC-3 and CWR22 tumors showed strong tumor-to-background contrast. **Conclusion:** This study demonstrates that PET imaging of ^{64}Cu-DOTA-[Lys^3]BBN is able to detect GRPR-positive prostate cancer.

Key Words: prostate cancer; microPET; gastrin-releasing peptide receptor; bombesin; ^{64}Cu

J Nucl Med 2004; 45:1390–1397

A high-resolution and high-sensitivity nuclear medicine technique using radiopharmaceuticals that depict physiologic, metabolic, and molecular processes in vivo is PET. The most widely used agent is ^{18}F-FDG, which accumulates in cells that have an increased metabolism due to increased need for or an inefficient glucose metabolism, such as cancer. Although ^{18}F-FDG PET has been shown to effectively detect many types of primary tumors and metastases, it is not able to reliably differentiate benign hyperplasia and prostate cancer (*1*) or even to detect organ-confined carcinoma (*2*). Uptake of ^{18}F-FDG in prostate carcinoma is generally low, apparently because the glucose utilization of prostate carcinoma cells is not enhanced significantly, compared with that of normal cells, to allow delineation of the tumor on the PET scan. Recent investigations of ^{11}C-labeled (*3,4*) and ^{18}F-labeled (*5–8*) choline and ^{11}C-acetate (*9–12*) indicate that these agents hold promise in this disease. High expression of receptors on prostate cancer cells, as compared with normal prostate tissue and peripheral blood cells, provides the molecular basis for using radiolabeled receptor agonists or antagonists to visualize prostate tumors in nuclear medicine. ^{18}F-Labeled androgens have been used to identify androgen-positive tissue in primates (*13*). Although this method is useful in determining if prostate cancer is hormone dependent, it does not provide a means for detecting tumors that are hormone independent. Thus, new markers that are able to identify the molecular determinants of prostate cancer development and progression regardless of androgen dependence need to be investigated.

The G protein–coupled gastrin-releasing peptide (GRP) receptor (GRPR) mediates the diverse actions of mammalian bombesin (BBN)-related peptide, GRP. In addition to

Received Dec. 1, 2003; revision accepted Feb. 5, 2004.

For correspondence or reprints contact: Peter S. Conti, MD, PhD, Department of Radiology, University of Southern California, 1510 San Pablo St., Suite 350, Los Angeles, CA 90033.

E-mail: pconti@usc.edu

its natural presence in the central nervous system and peripheral tissues, GRPR is overexpressed in several neuroendocrine tumors, including prostate cancer (*14,15*). In vitro receptor autoradiography of human nonneoplastic and neoplastic prostate tissue sections with ^{125}I-[Tyr^4]BBN as radioligand indicated high density of GRPR in well-differentiated carcinomas as well as bone metastases, but little or no GRPR was found in hyperplastic prostate and glandular tissue. This suggests that GRPR may be an indicator of early molecular events in prostate carcinogenesis and may be useful in differentiating prostate hyperplasia from neoplasia (*14,15*). GRPR-specific binding of ^{125}I-[Tyr^4]BBN was observed in human prostate cancer cell lines that are androgen independent (AI) but not in those that are androgen dependent (AD) (*16*). GRP promotes the growth and invasiveness of prostate cancer in vitro, and its secretion in vivo by endocrine cells is thought to be partially responsible for AI progression of the disease (*17*) by transactivation and upregulation of epidermal growth factor receptors (*18*). Therefore, the use of GRPR antagonists or GRPR-targeting cytotoxic peptide conjugates could be an effective chemotherapeutic approach (*19*). In nuclear medicine, suitably radiolabeled BBN analogs have great potential for early noninvasive diagnosis as well as radiotherapy of prostate cancer (*20,21*).

γ-Emitting ^{99m}Tc-labeled BBN analogs have been synthesized and evaluated in vivo in normal mice (*22,23*) and PC-3 tumor-bearing mice (*24,25*) and have undergone feasibility testing in human patients (*21*). Although γ-emitters currently are more readily available relative to positron-emitting radionuclides (β^+), the sensitivity of PET is at least 1–2 orders of magnitude better than that of single photon imaging systems (*26*). The acquisition of higher count statistics permits detection of smaller tumors for a given amount of radioactivity.

Recently, Rogers et al. (*27*) labeled DOTA-Aoc-BBN(7–14) (Aoc is 8-aminooctanoic acid) with ^{64}Cu and applied this radiotracer to subcutaneous PC-3 xenografts. Although the tumor was well visualized, the sustained blood concentration and persistent liver and kidney retention limited potential clinical application of this tracer. In the present work, we evaluated the DOTA-[Lys^3]BBN conjugate (DOTA is 1,4,7,10-tetraazadodecane-*N*,*N*′,*N*″,*N*‴-tetraacetic acid) complexed with ^{64}Cu for in vitro receptor-binding assay in PC-3 cells, for tumor targeting and in vivo kinetics by direct tissue sampling, and for visualization of prostate cancer tumors by microPET and whole-body autoradiography.

MATERIALS AND METHODS

Chemistry and Radiochemistry

[Lys^3]BBN (American Peptide, Inc.) was conjugated with DOTA via in situ activation and coupling. Typically, DOTA, 1-ethyl-3-[3-(dimethylamino)propyl]carbodiimide (EDC), and *N*-hydroxysulfonosuccinimide (SNHS) at a molar ratio of DOTA:EDC:SNHS = 10:5:4 were mixed and reacted at 4°C for 30 min (pH = 5.5). The sulfosuccinimidyl ester of DOTA (DOTA-OSSu) prepared without purification was then reacted with [Lys^3]BBN in a theoretic stoichiometry of 5:1 and allowed to stand at 4°C overnight (pH 8.5–9.0). The DOTA-[Lys^3]BBN conjugate was then purified by semipreparative high-performance liquid chromatography (HPLC) using a Waters 515 chromatography system with a Vydac protein and peptide column (218TP510; 5 μm, 250 × 10 mm). The flow was 3 mL/min, with the mobile phase starting from 95% solvent A (0.1% trifluoroacetic acid [TFA] in water) and 5% solvent B (0.1% TFA in acetonitrile) (0–2 min) to 35% solvent A and 65% solvent B at 32 min. The peak containing the DOTA conjugate was collected, lyophilized, and dissolved in H_2O at a concentration of 1 mg/mL for use in radiolabeling reactions. Analytic HPLC was performed on the same pump system using a Vydac 218TP54 column (5 μm, 250 × 4.6 mm) and flow rate of 1 mL/min.

^{64}Cu was produced on a CS-15 biomedical cyclotron at Washington University School of Medicine. The DOTA-[Lys^3]BBN conjugate was labeled with ^{64}Cu by addition of 37–185 MBq (1–5 mCi) ^{64}Cu (2–5 μg DOTA-[Lys^3]BBN conjugate per MBq ^{64}Cu) in 0.1N NaOAc (pH 5.5) buffer followed by a 45-min incubation at 50°C. The reaction was terminated by adding 5 μL of 10 mmol/L ethylenediaminetetraacetic acid solution, and radiochemical yield was determined by radio-TLC (TLC = thin-layer chromatography) using Whatman MKC18F TLC plates as the stationary phase and 70:30 MeOH:10% NaOAc as the eluent. ^{64}Cu-DOTA-RGD was purified on a C_{18} SepPak cartridge, using 85% ethanol as the elution solvent. Radiochemical purity was determined by radio-TLC or radio-HPLC. The ethanol was evaporated and the activity was reconstituted in phosphate-buffered saline and passed through a 0.22-μm Millipore filter into a sterile multidose vial for in vitro and animal experiments.

In Vitro Receptor-Binding Studies

In vitro GRPR-binding affinities and specificities of the DOTA-[Lys^3]BBN conjugate were assessed via displacement cell-binding assays using ^{125}I-[Tyr^4]BBN (Perkin-Elmer Life Sciences Products, Inc.) as the GRPR-specific radioligand. Experiments were performed on PC-3 (AI) human prostate cancer cells (American Type Culture Collection) by modification of a method previously described (*25*). Briefly, cells were grown in Ham's F-12K medium supplemented with 10% fetal bovine serum. PC-3 cells were harvested and seeded in 24-well plates at 10^5 cells per well. Twenty-four hours later, the cells were washed twice with binding buffer containing 50 mmol/L *N*-(2-hydroxyethyl)piperazine-*N*′-(2-ethanesulfonic acid, 125 mmol/L NaCl, 7.5 mmol/L KCl, 5.5 mmol/L $MgCl_2$, 1 mmol/L ethylene glycol-bis-(β-aminoethyl-ester)-*N*,*N*,*N*′,*N*′-tetraacetic acid, 2 mg/mL bovine serum albumin, 2 mg/L chymostatin, 100 mg/L soybean trypsin inhibitor, and 50 mg/L bacitracin at pH 7.4 and then incubated for 1 h at 37°C with 20,000 cpm of ^{125}I-[Tyr^4]BBN (specific activity, 74 TBq/mmol [2,000 Ci/mmol]) in the presence of increasing concentrations of DOTA-[Lys^3]BBN conjugate ranging from 0 to 2,000 nmol/L. After incubation, the cells were washed twice with binding buffer and solubilized with 1N NaOH, and activity was measured in a γ-counter (Packard). The 50% inhibitory concentration (IC_{50}) value for the displacement binding of ^{125}I-[Tyr^4]BBN by DOTA-[Lys^3]BBN conjugate was calculated by nonlinear regression analysis using the GraphPad Prism computer-fitting program (GraphPad Software, Inc.). Experiments were done twice with triplicate samples.

Internalization Studies

Internalization of ^{64}Cu-DOTA-[Lys^3]BBN was measured by modifying a previously described technique (*25*). Briefly, PC-3 (AI) cells were incubated in triplicate in 6-well plates with about 200,000 cpm of ^{64}Cu-labeled tracer with or without an excess of 1 μmol/L BBN for 2 h at 4°C. After the preincubation, cells were washed with ice-cold binding buffer to remove free radioligand and then incubated with previously warmed binding buffer at 37°C for 0, 15, 30, and 120 min for internalization. The percentage of ^{64}Cu activity trapped in the cells was determined after removing ^{64}Cu activity bound to the cell surface by washing twice with acid (50 mmol/L glycine and 0.1 mol/L NaCl, pH 2.8). Cells were then solubilized by incubating with 1N NaOH and counted to determine internalized radioligand.

Biodistribution

Human prostate cancer carcinoma xenografts were induced by subcutaneous injection of 10^7 PC-3 (AI) cells to the left front leg and 10^7 CWR22 (AD) cells to the right front leg of 4- to 6-wk-old male athymic nude mice (Harlan). Three to 4 wk later, when the tumors reached 0.4- to 0.6-cm diameter, the mice were injected with 370 kBq (10 μCi) DOTA-[Lys^3]BBN intravenously into the tail vein. Mice (n = 4 per time point) were killed by cervical dislocation at different time points after injection. Blood, tumor, and the major organs and tissues were collected, wet weighed, and counted in a γ-counter (Packard). The percentage of injected dose per gram (%ID/g) was determined for each sample. For each mouse, radioactivity of the tissue samples was calibrated against a known aliquot of the injectate. Values are expressed as mean ± SD. The receptor-mediated localization of the radiotracers was investigated by determining the biodistribution of radiolabeled peptide in the presence of 1 and 10 mg/kg of BBN at 1 h after injection (n = 4).

microPET Imaging

PET imaging was performed on a microPET R4 rodent model scanner (Concorde Microsystems, Inc.). The scanner has a computer-controlled bed, 10.8-cm transaxial and 8-cm axial field of view (FOV). It has no septa and operates exclusively in 3-dimensional list mode. All raw data were first sorted into 3-dimensional sinograms, followed by Fourier rebinning and 2-dimensional filtered backprojection image reconstruction using a ramp filter with the Nyquist limit (0.5 cycle/voxel) as the cutoff frequency. For PET imaging of prostate cancer-bearing mice, the animals were injected with 14.8 MBq (400 μCi) ^{64}Cu-DOTA-[Lys^3]BBN via the tail vein. Each mouse was then killed at 1 h after injection and placed near the center of the FOV of the microPET, where the highest image resolution and sensitivity are available. Static imaging was performed for 20 min (n = 3). For a receptor-blocking experiment, one mouse bearing PC-3 tumor on the right front leg was imaged (20-min static scan at 1 h after administration of 14.8 MBq [400 μCi] ^{64}Cu-DOTA-[Lys^3]BBN) twice 2 d apart: (a) without coinjection with BBN; and (b) with 10 mg/kg BBN. No attenuation correction was applied to the microPET scans. Instead, the attenuation correction factors were incorporated into the system calibration. In brief, a vial with a volume (30 mL, 5-cm diameter) similar to that of a nude mouse body was filled with a known amount of $^{64}CuCl_2$ and scanned for 1 h. The static scan was reconstructed with the filtered backprojection protocol, and the counting rate from the images of the phantom was compared with the known activity concentration to obtain a system calibration factor. With this approach, the uptake index (ROI [kBq/mL]/injected dose [kBq] × 100%, where ROI = region of interest) of tissues and of organs of interest was consistent with the %ID/g value obtained from direct tissue sampling after the microPET imaging. The error was within 5%–10%.

Whole-Body Autoradiography

Autoradiography was performed using a Packard Cyclone Storage Phosphor Screen system and a Bright 5030/WD/MR cryomicrotome (Hacker Instruments). Immediately after microPET scanning, the mice were frozen in a dry ice and isopropyl alcohol bath for 2 min. The bodies were then embedded in a 4% carboxymethyl cellulose (Aldrich) water mixture using a stainless steel and aluminum mold. The mold was placed in the dry ice and isopropyl alcohol bath for 5 min and then into a −20°C freezer for 1 h. The walls of the mold were removed, and the frozen block was mounted in the cryomicrotome. The block was cut into 50-μm sections, and desired sections were digitally photographed and captured for autoradiography. The sections were transferred into a chilled autoradiography cassette containing a Super Resolution Screen (Packard) and kept there overnight at −20°C. Screens were read with the Packard Cyclone laser scanner. Quantification of autoradiographic images was validated by a direct tissue sampling technique. In brief, 50-μm slices of tumor tissue were cut and exposed to the Super Resolution Screen for 24 h, and the ROIs drawn from the autoradiographs were described as detector light units per mm^2 and correlated with direct γ-counter assays of the tissue samples scooped out of the frozen block (n = 3). A linear relationship between tissue %ID/g and autoradiography image intensity was obtained, and the conversion factor thus obtained was used for autoradiography quantification.

Statistic Analysis

Data are expressed as mean ± SD. One-way ANOVA was used for statistical evaluation. Means were compared using the Student t test. P values < 0.05 were considered significant.

RESULTS

Synthesis and Radiolabeling

The DOTA-[Lys^3]BBN conjugate (Fig. 1) was produced in 75% yield after HPLC purification. The retention time of this compound on HPLC was 18.5 min, whereas [Lys^3]BBN eluted at 19.2 min under the same conditions. Matrix-assisted laser desorption ionization–time of flight mass spectrometry (MALDI-TOF MS): m/z = 1,976 for $[M+H]^+$ ($C_{87}H_{137}N_{26}O_{26}S$); 1,998 for $[M+Na]^+$; and 2,014 for $[M+K]^+$. ^{64}Cu-DOTA-[Lys^3]BBN was labeled in ≥90% radiochemical yield and ≥98% radiochemical purity and was used immediately for in vitro and in vivo assays. Free ^{64}Cu-acetate remained at the origin of the radio-TLC plate and the R_f value of ^{64}Cu-DOTA-[Lys^3]BBN was about 0.5. The specific activity of ^{64}Cu-DOTA-RGD ranged from 15 to 38 GBq/μmol (400–1,000 Ci/mmol).

In Vitro Receptor-Binding Assay

The binding affinity of DOTA-[Lys^3]BBN conjugate for GRPR was tested for AI human prostate cancer PC-3 cells. As seen in Figure 2, the data show a typical sigmoid curve for the displacement of ^{125}I-[Tyr^4]BBN from PC-3 cells as a function of increasing concentrations of the DOTA-

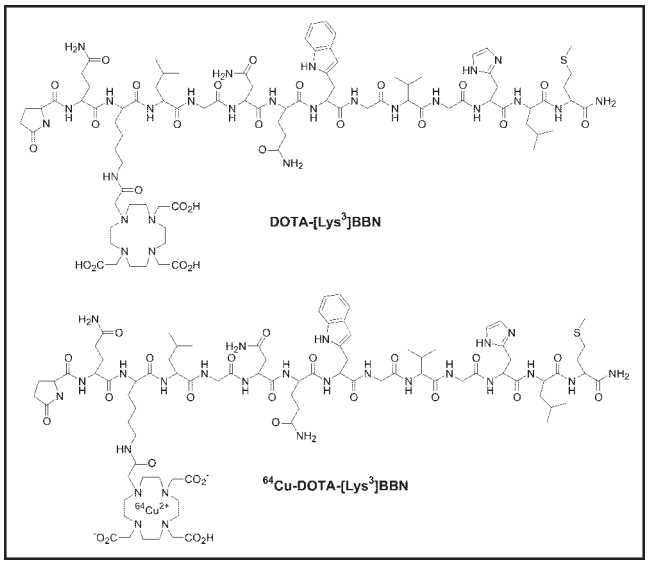

FIGURE 1. Schematic structures of DOTA-[Lys^3]BBN conjugate and ^{64}Cu-DOTA-[Lys^3]BBN.

[Lys^3]BBN conjugate. The IC_{50} value was determined to be 2.2 ± 0.5 nmol/L. In the absence of DOTA-[Lys^3]BBN competitor, approximately 10% of added ^{125}I-[Tyr^4]BBN was bound. Only about 1% of added radioligand was bound to the cells in the presence of 1 μmol/L of DOTA-[Lys^3]BBN, suggesting that 90% of bound ^{125}I-[Tyr^4]BBN was GRPR specific.

The internalization of ^{64}Cu-DOTA-[Lys^3]BBN into PC-3 cells is illustrated in Figure 3. The rate of internalization was time and temperature dependent. At 4°C, cell surface binding occurred but internalization was minimal (<10%). Incubation at 37°C showed a rapid internalization rate, with 65% ± 10% of radioactivity internalized by 30 min.

Biodistribution Studies

A summary of the biodistribution data for ^{64}Cu-DOTA-[Lys^3]BBN in PC-3 and CWR22 tumor-bearing mice is shown in Figure 4. This radiotracer had a rapid blood clearance, with only 0.30 ± 0.04 %ID/g remaining in the circulation at 1 h followed by a further decrease at 2 and 4-h time points. Tumor-to-blood ratios at 1 h were 13.1 ± 2.3 and 4.1 ± 1.3 for PC-3 and CWR22 tumors, respectively. Liver uptake reached maximum at 1 h (4.18 ± 0.63 %ID/g) and declined to 2.09 ± 0.5 %ID/g at 2 h after injection. The rapid decrease of activity accumulation in the kidneys suggests a predominant renal clearance pathway of this radiotracer. A significant uptake of ^{64}Cu-DOTA-[Lys^3]BBN in the GRPR-bearing pancreas was observed (10.4 ± 0.14 %ID/g at 30 min after injection and 6.08 ± 0.18 %ID/g after 2 h). Our results indicated GRPR-specific uptake in PC-3 tumor and pancreas (Fig. 5), which was confirmed by the receptor-blocking study at the 1-h time point, as the uptake in these tissues was effectively inhibited by coinjection of 10 mg/kg BBN (7.83 ± 0.52 %ID/g vs. 0.52 ± 0.05 %ID/g for pancreas, $P < 0.001$; 3.97 ± 0.15 %ID/g vs. 1.35 ± 0.24 %ID/g for PC-3 tumor, $P < 0.001$). Coinjection of 1 mg/kg BBN resulted in partial inhibition of activity accumulation in PC-3 tumor (2.08 ± 0.35 %ID/g) and pancreas (2.75 ± 0.43 %ID/g). Activity accumulation in the AD CWR22 tumor was not affected by the administration of BBN. No significant changes of uptake in other normal organs were seen except for the kidneys, which had increased uptake in the blocked versus the control mice ($P < 0.01$), presumably due to decreased specific binding in tissues.

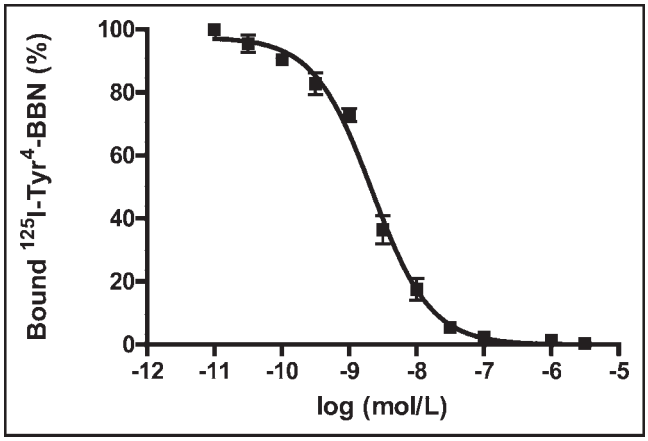

FIGURE 2. Inhibition of ^{125}I-[Tyr^3]BBN binding to GRPR on human prostate cancer cell line PC-3 by DOTA-[Lys^3]BBN conjugate (IC_{50} = 2.2 ± 0.5 nmol/L). Results expressed as percentage of binding are mean ± SD of 2 experiments in triplicate.

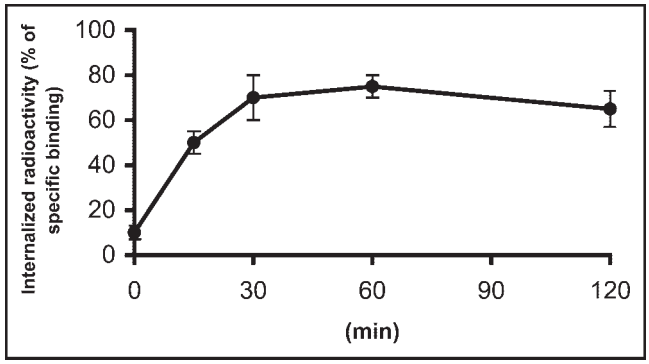

FIGURE 3. Time-dependent internalization of ^{64}Cu-DOTA-[Lys^3]BBN by PC-3 prostate cancer cells incubated at 37°C during 2 h. Cells were preincubated for 2 h at 4°C. Data are mean ± SD of percentage of acid-resistant (internalized) radioactivity in cells (2 experiments in triplicate).

microPET and Autoradiographic Imaging

The localization of ^{64}Cu-DOTA-[Lys^3]BBN in PC-3 and CWR22 tumor-bearing mice as determined by microPET imaging followed by whole-body autoradiography is depicted in Figure 6. On the left is a coronal image of a tumor-bearing mouse 1 h after administration of 14.8 MBq (400 μCi) ^{64}Cu-DOTA-[Lys^3]BBN. The microPET image is concordant with a whole-body autoradiographic section seen on the right. Both PC-3 (left) and CWR22 (right) tumors were visible with clear contrast from the adjacent background. Prominent uptake was also observed in the

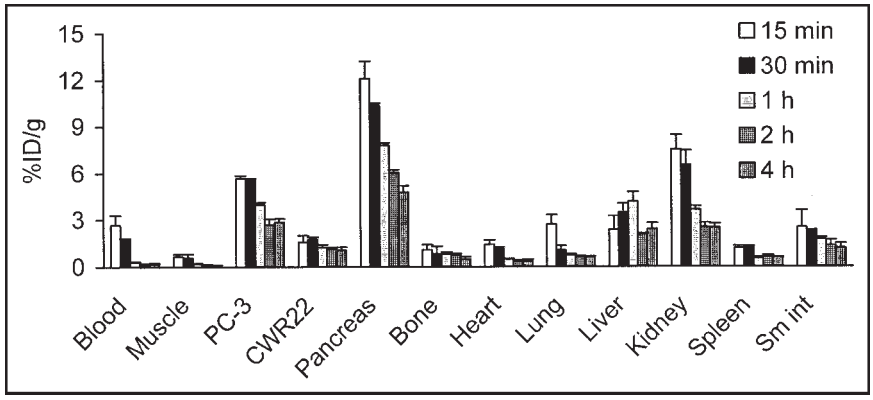

FIGURE 4. Biodistribution of ^{64}Cu-DOTA-[Lys^3]BBN in male athymic nude mice bearing subcutaneous PC-3 (AI) and CWR22 (AD) tumors. Mice were intravenously injected with 370 kBq (10 μCi) of radioligand and killed at 15 min, 30 min, 1 h, 2 h, and 4 h. Data are presented as mean %ID/g ± SD (n = 4). Sm int = small intestine.

liver and kidneys, and clearance of the activity through the urinary bladder is evident. Uptake indices at 1 h derived from microPET (tail vein injection of 14.8 MBq [400 μCi] activity) and quantitative autoradiography (QAR) are compared with data obtained from direct tissue sampling (tail vein injection of 370 kBq [10 μCi] activity) in Figure 7. The results from microPET ROI analysis agreed with the results obtained from autoradiographic quantification for the organs and tissues examined. It is evident that PC-3 tumor and pancreas uptake obtained from microPET and QAR were significantly lower than those obtained from the direct biodistribution measurement. Figure 8 shows transaxial microPET images of a PC-3 tumor-bearing nude mouse, 1 h after administration of ^{64}Cu-DOTA-[Lys^3]BBN, with and without coinjection of 10 mg/kg BBN. There is a clear visualization of the PC-3 tumor in the animal on the left without the presence of competitor. Conversely, the same mouse that received a blocking dose of BBN showed reduced tracer localization in the tumor.

DISCUSSION

This study showed that suitably labeled BBN analogs can be used to image both AI and AD prostate cancer in preclinical animal models. In particular, this study demonstrated that AI PC-3 but not AD CWR22 prostate cancer tumor has GRPR-specific activity accumulation.

The overexpression of peptide receptors in human tumors is of considerable interest for tumor imaging and therapy. Because of their small size, peptides have faster blood clearance and higher target-to-background ratios compared with those of macromolecular compounds. Radiolabeled receptor-binding peptides have recently emerged as a new class of radiopharmaceuticals. Various peptides have been used for tumor scintigraphy. For example, somatostatin receptors, which are highly expressed in most neuroendocrine tumors, have been targeted successfully for both imaging and therapy with octreotide. The long-term treatment of patients with octreotide has been successful in relieving the symptoms resulting from excessive hormone production by the tumors (*28*). The use of radiolabeled somatostatin analogs has permitted imaging as well as therapy of neuroendocrine tumors and their metastases in patients (*29*). Similar targeting strategies have also been applied to vasoactive intestinal peptide receptors in epithelial tumors (*30*) and cholecystokinin-B receptors in medullary thyroid car-

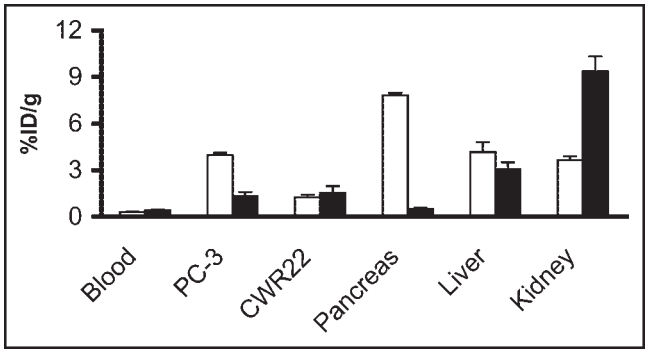

FIGURE 5. Receptor-blocking study: biodistribution of ^{64}Cu-DOTA-[Lys^3]BBN at 1-h time point without (white bars) and with (black bars) coinjection of 200 μg of BBN to determine GRPR-specific binding. Significant inhibition of activity accumulation in PC-3 tumor ($P < 0.001$) and pancreas ($P < 0.001$) was observed. Data are presented as mean %ID/g ± SD in reference to total injected dose of radiotracer (n = 4 for each group).

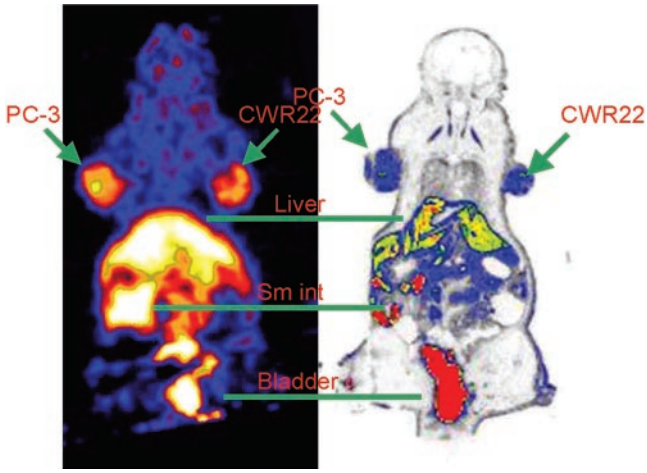

FIGURE 6. (Left) Coronal microPET image of tumor-bearing mouse (PC-3 on left shoulder and CWR22 on right shoulder) 1 h after administration of ^{64}Cu-DOTA-[Lys^3]BBN. (Right) Digital autoradiograph of section containing tumors.

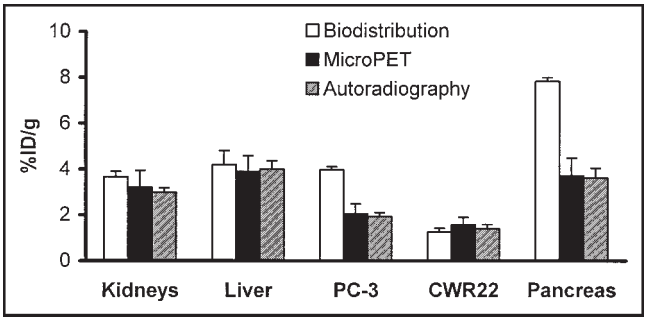

FIGURE 7. Kidney, liver, PC-3 tumor, and CWR22 tumor uptake comparison as obtained from traditional biodistribution (n = 4), microPET (n = 3), and autoradiographic quantification (n = 3). Quantification of microPET and autoradiography revealed similar activity accumulation in both PC-3 tumor and pancreas, which were both lower than those obtained from biodistribution study.

cinomas and small cell lung cancers (*31*). Recently, we and other groups have labeled cyclic RGD peptides with various radionuclides for imaging of tumor angiogenesis (*32*,*33*). Overexpression of the GRPR in a variety of neoplasias, such as breast, prostate, pancreatic, and small cell lung cancers, was prompted by the development of γ-emitting or positron-emitting radionuclide-labeled GRP analogs for SPECT (*20*–*25*,*34*) and PET (*27*) imaging of GRPR-positive tumors.

Since the native BBN peptide has a pyroglutamic acid at the N-terminus and an amidated methionine at the C-terminus, further modification and radiolabeling of this peptide with metallic radionuclides is not possible. Efforts have been made to design derivatized BBN analogs for binding and pharmacokinetic studies. Because BBN agonists are generally preferable to BBN antagonists for receptor-specific internalization, most BBN analogs with an amidated C-terminus that have been developed are agonists. Because the C-terminus is directly involved in the specific binding interaction with the GRPR, the truncated C-terminal heptapeptide sequence Trp-Ala-Val-Gly-His-Leu-Met (BBN(8–14)) must be maintained or minimally substituted. Several strategies have been applied to develop radiometallated BBN-analogous conjugates. For example, the N-terminal Glp of BBN has been replaced by Pro and subsequently conjugated with DOTA and diethylenetriaminepentaacetic acid (DTPA) for ^{111}In labeling (*35*,*36*); Arg^3 was substituted with Lys^3 and a N_2S_2 ligand was attached to the Lys side chain ϵ-amino group for ^{99m}Tc labeling (*22*) or DOTA and DTPA were attached to Lys^3 of [Lys^3,Tyr^4]BBN for ^{111}In labeling (*35*). Most of the studies reported to date used a C-terminal amidated BBN(8–14) in which radiometal chelate was linked to the truncated small peptide (*37*,*38*) for ^{99m}Tc labeling[b]. Recently, Rogers et al. (*27*) reported ^{64}Cu-labeled, DOTA-conjugated, Aoc linker-modified BBN(7–14) for microPET imaging of subcutaneous PC-3 tumor models. The strategy used in our laboratory has focused primarily on modification of the Lys^3 residue of [Lys^3]BBN with various linkers and chelators for diagnostic and therapeutic applications. This study reports ^{64}Cu-labeled DOTA-[Lys^3]BBN for microPET imaging of both AI and AD tumor models.

In contrast to many other investigators who tried to conjugate DOTA chelator to peptides via solid-phase synthesis using DOTA-tris(*t*-butyl ester) followed by TFA cleavage and deprotection, we found that the incorporation yield of tri-*t*-butyl ester–protected DOTA to fully protected peptides fixed on resin was low due to steric hindrance of the bulky protecting groups. Purification of the peptide conjugates was difficult due to the fact that DOTA-peptide conjugates usually had a retention time similar to those of the parent peptides. We also found it more convenient to prepare DOTA-peptide conjugates in buffer solutions via in situ activation of DOTA. The retention time of DOTA-[Lys^3]BBN is different from that of [Lys^3]BBN by $<$1 min under the HPLC condition in this study. However, the use of an excess amount of DOTA for conjugation resulted in almost complete conversion of [Lys^3]BBN to DOTA-[Lys^3]BBN. The radiolabeling of DOTA-[Lys^3]BBN with ^{64}Cu was performed with high yield. Unreacted ^{64}Cu was easily removed by simple C_{18} cartridge elution.

DOTA-[Lys^3]BBN had high affinity for the GRPR (IC_{50} = 2.2 ± 0.5 nmol/L; Fig. 2) similar to that of BBN (1.5 nmol/L) (*25*). This study agrees with the findings by Baidoo et al. (*22*) that modification of the Lys^3 ϵ-amino group has little effect on the receptor-binding characteristics of the peptide. ^{64}Cu-Labeled DOTA-[Lys^3]BBN was rapidly internalized by PC-3 cells, consistent with the expected agonistic behavior of this radiotracer against GRPR. Maximum internalization and retention of the radioactivity by tumor cells is needed for diagnostic or therapeutic efficacy of radiopharmaceuticals. There was limited efflux of ^{64}Cu activity from the PC-3 cells within the period of investigation (2 h), presumably due to residualization of ^{64}Cu from GRPR-mediated entrapment of the tracer in lysosomes (*39*,*40*) and subsequent degradation by lysosomal proteases. Similar results have been obtained with other radiolabeled BBN analogs.

Biodistribution studies were performed on both PC-3 (AI) and CWR22 (AD) tumor-bearing mice. It has been

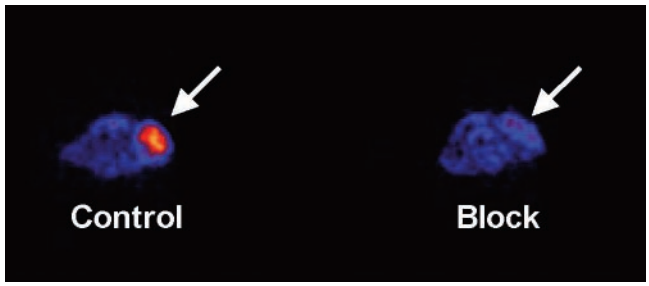

FIGURE 8. Transaxial microPET images of athymic nude mouse bearing PC-3 tumor on right shoulder 1 h after tail vein injection of 14.8 MBq (400 μCi) ^{64}Cu-DOTA-[Lys^3]BBN in absence (control) and presence (block) of coinjected blocking dose of BBN (10 mg/kg). Arrows indicate location of tumors.

reported that AI tumor cells express GRPRs at significantly higher levels than do AD tumor cells (*16*). In the current study, activity accumulation from ^{64}Cu-DOTA-[Lys^3]BBN by AI PC-3 tumors was significantly higher than by AD CWR22 tumors. It is interesting to note that receptor blocking did not reduce the uptake in CWR22 tumor, whereas the activity in GRPR-positive PC-3 tumor and pancreas were effectively inhibited. Fast blood clearance of radiotracer after 30 min following administration might have been due to little binding of the degradation metabolites to plasma proteins. This is very different from the in vivo behavior of ^{64}Cu-DOTA-Aoc-BBN(7–14) (*27*), which exhibited persistent blood retention up to 24 h after injection and higher normal tissue uptake than that reported in this and other studies. A high degree of plasma protein binding of the relatively lipophilic Aoc linker as well as transchelation of Cu^{2+} to albumin and superoxide dismutase may have caused the unfavorably high liver activity accumulation. Smith et al. (*38*) also reported that a long aliphatic linker is responsible for prolonged retention in blood and decreased pancreatic uptake.

Although ^{99m}Tc-labeled GRP analogs have receptor-specific tumor activity accumulation, the absolute tumor uptake is rather low (<1%ID/g at 1 h after injection). ^{64}Cu-Labeled BBN analogs reported here and by Rogers et al. (*27*) gave much higher tumor uptake and more persistent tumor retention. Further investigations are needed to fully understand the effect of radiochelate characteristics, linker properties, and peptide sequences on tumor-targeting ability and excretion kinetics. As opposed to ^{64}Cu-DOTA-Aoc-BBN(7–14), which had both hepatobiliary and renal excretion pathways, ^{64}Cu-DOTA-[Lys^3]BBN was excreted rapidly via the renal route. This suggests that insertion of a rather hydrophobic aliphatic acid linker to separate the radiolabel from the receptor-targeting peptide moiety is probably not beneficial for optimization of such radioligands.

microPET imaging of ^{64}Cu-DOTA-[Lys^3]BBN in mice bearing both AI PC-3 and AD CWR22 tumors 1 h after injection of radioactivity revealed a high tumor-to-background ratio for both tumor types (Fig. 6). The uptake indices found with microPET and QAR for PC-3 tumor and pancreas were significantly lower than those obtained from direct tissue sampling (Fig. 7). Assuming the specific activity of the radiotracer was 18.5 GBq/μmol (500 mCi/μmol) at the time of tail vein injection, the injection administered for microPET imaging contained about 2 μg BBN peptide (14.8 MBq [400 μCi]), whereas the amount of activity administered for the biodistribution experiment contained only 50 ng BBN peptide (370 kBq [10 μCi]). It is possible that partial self-inhibition of receptor-specific uptake in PC-3 tumor, pancreas, and other tissues that express the GRPR occurred during the imaging studies. Conversely, the inability to inhibit CWR22 tumor activity accumulation in the imaging study is consistent with the known low GRPR expression in AD tumors such as CWR22 (*16*).

We anticipate that quantitative imaging with microPET in living animals, based on the overexpression of GRPR in invasive prostate cancer, could potentially be translated into clinical settings to detect AI prostate cancer. Successful targeting of this molecular pathway would have diagnostic as well as potential radio- and chemotherapeutic implications: the ability to document GRPR density and the appropriate selection of patients entering clinical trials for anti-GRPR treatment. PET imaging of prostate cancer with ^{64}Cu-labeled BBN analogs also will be useful for determining dosimetry and tumor response to the same ligand labeled with therapeutic amounts of ^{67}Cu for internal radiotherapy.

CONCLUSION

[Lys^3]BBN, when conjugated with a macrocyclic DOTA-chelating group and radiolabeled with the positron-emitting radionuclide ^{64}Cu, exhibits high GRPR-binding affinity and specificity and rapid internalization in AI PC-3 prostate cancer cells. Specific localization of ^{64}Cu-DOTA-[Lys^3]BBN to PC-3 tumor and GRPR-positive tissues was confirmed by biodistribution, microPET imaging, and autoradiographic imaging studies. Reduced tumor uptake in PC-3 tumor but not CWR22 tumor in high-dose microPET and autoradiography studies compared with low-dose biodistribution studies further illustrates high-affinity and low-capacity characteristics of the GRPR in AI tumors. The activity accumulation in CWR22 tumor is attributed to nonspecific uptake. Further studies to evaluate the metabolic stability and optimization of the radiotracers for prolonged tumor retention and improved in vivo kinetics are necessary.

ACKNOWLEDGMENTS

This work was funded by the Department of Defense Prostate Cancer Research Program DAMD17-03-1-0143 and National Institutes of Health grant P20 CA86532. Production of ^{64}Cu at Washington University School of Medicine was supported by National Cancer Institute grant R24 CA86307.

REFERENCES

1. Effert PJ, Bares R, Handt S, Wolff JM, Bull U, Jakse G. Metabolic imaging of untreated prostate cancer by positron emission tomography with ^{18}F-labeled deoxyglucose. *J Urol.* 1996;155:994–998.
2. Liu IJ, Zafar MB, Lai YH, Segall GM, Terris MK. Fluorodeoxyglucose positron emission tomography studies in diagnosis and staging of clinically organ-confined prostate cancer. *Urology.* 2001;57:108–111.
3. Hara T, Kosaka N, Kishi H. PET imaging of prostate cancer using carbon-11-choline. *J Nucl Med.* 1998;39:990–995.
4. Kotzerke J, Prang J, Neumaier B, et al. Experience with carbon-11 choline positron emission tomography in prostate carcinoma. *Eur J Nucl Med.* 2000;27:1415–1419.
5. Price DT, Coleman RE, Liao RP, Robertson CN, Polascik TJ, DeGrado TR. Comparison of [^{18}F]fluorocholine and [^{18}F]fluorodeoxyglucose for positron emission tomography of androgen dependent and androgen independent prostate cancer. *J Urol.* 2002;168:273–280.
6. DeGrado TR, Baldwin SW, Wang S, et al. Synthesis and evaluation of ^{18}F-labeled choline analogs as oncologic PET tracers. *J Nucl Med.* 2001;42:1805–1814.

7. DeGrado TR, Coleman RE, Wang S, et al. Synthesis and evaluation of ^{18}F-labeled choline as an oncologic tracer for positron emission tomography: initial findings in prostate cancer. *Cancer Res.* 2001;61:110–117.
8. Hara T, Kosaka N, Kishi H. Development of ^{18}F-fluoroethylcholine for cancer imaging with PET: synthesis, biochemistry, and prostate cancer imaging. *J Nucl Med.* 2002;43:187–199.
9. Kotzerke J, Volkmer BG, Neumaier B, Gschwend JE, Hautmann RE, Reske SN. Carbon-11 acetate positron emission tomography can detect local recurrence of prostate cancer. *Eur J Nucl Med Mol Imaging.* 2002;29:1380–1384.
10. Kato T, Tsukamoto E, Kuge Y, et al. Accumulation of [^{11}C]acetate in normal prostate and benign prostatic hyperplasia: comparison with prostate cancer. *Eur J Nucl Med Mol Imaging.* 2002;29:1492–1495.
11. Oyama N, Akino H, Kanamaru H, et al. ^{11}C-Acetate PET imaging of prostate cancer. *J Nucl Med.* 2002;43:181–186.
12. Oyama N, Miller TR, Dehdashti F, et al. ^{11}C-Acetate PET imaging of prostate cancer: detection of recurrent disease at PSA relapse. *J Nucl Med.* 2003;44:549–555.
13. Bonasera TA, O'Neil JP, Xu M, et al. Preclinical evaluation of fluorine-18-labeled androgen receptor ligands in baboons. *J Nucl Med.* 1996;37:1009–1015.
14. Markwalder R, Reubi JC. Gastrin-releasing peptide receptors in the human prostate: relation to neoplastic transformation. *Cancer Res.* 1999;59:1152–1159.
15. Sun B, Halmos G, Schally AV, Wang X, Martinez M. Presence of receptors for bombesin/gastrin-releasing peptide and mRNA for three receptor subtypes in human prostate cancers. *Prostate.* 2000;42:295–303.
16. Reile H, Armatis PE, Schally AV. Characterization of high-affinity receptors for bombesin/gastrin releasing peptide on the human prostate cancer cell lines PC-3 and DU-145: internalization of receptor bound ^{125}I-(Tyr^4) bombesin by tumor cells. *Prostate.* 1994;25:29–38.
17. Jongsma J, Oomen MH, Noordzij MA, et al. Androgen-independent growth is induced by neuropeptides in human prostate cancer cell lines. *Prostate.* 2000;42:34–44.
18. Szepeshazi K, Halmos G, Schally AV, et al. Growth inhibition of experimental pancreatic cancers and sustained reduction in epidermal growth factor receptors during therapy with hormonal peptide analogs. *J Cancer Res Clin Oncol.* 1999;125:444–452.
19. Schally AV, Comaru-Schally AM, Plonowski A, Nagy A, Halmos G, Rekasi Z. Peptide analogs in the therapy of prostate cancer. *Prostate.* 2000;45:158–166.
20. Van de Wiele C, Dumont F, Dierckx RA, et al. Biodistribution and dosimetry of ^{99m}Tc-RP527, a gastrin-releasing peptide (GRP) agonist for the visualization of GRP receptor-expressing malignancies. *J Nucl Med.* 2001;42:1722–1727.
21. Van de Wiele C, Dumont F, Vanden Broecke R, et al. Technetium-99m RP527, a GRP analogue for visualisation of GRP receptor-expressing malignancies: a feasibility study. *Eur J Nucl Med.* 2000;27:1694–1699.
22. Baidoo KE, Lin KS, Zhan Y, Finley P, Scheffel U, Wagner HN Jr. Design, synthesis, and initial evaluation of high-affinity technetium bombesin analogues. *Bioconjug Chem.* 1998;9:218–225.
23. Karra SR, Schibli R, Gali H, et al. ^{99m}Tc-Labeling and in vivo studies of a bombesin analogue with a novel water-soluble dithiadiphosphine-based bifunctional chelating agent. *Bioconjug Chem.* 1999;10:254–260.
24. La Bella R, Garcia-Garayoa E, Langer M, Blauenstein P, Beck-Sickinger AG, Schubiger PA. In vitro and in vivo evaluation of a ^{99m}Tc(I)-labeled bombesin analogue for imaging of gastrin releasing peptide receptor-positive tumors. *Nucl Med Biol.* 2002;29:553–560.
25. La Bella R, Garcia-Garayoa E, Bahler M, et al. A ^{99m}Tc(I)-postlabeled high affinity bombesin analogue as a potential tumor imaging agent. *Bioconjug Chem.* 2002;13:599–604.
26. Wu AM, Yazaki PJ, Tsai S, et al. High-resolution microPET imaging of carcinoembryonic antigen-positive xenografts by using a copper-64-labeled engineered antibody fragment. *Proc Natl Acad Sci USA.* 2000;97:8495–8500.
27. Rogers BE, Bigott HM, McCarthy DW, et al. MicroPET imaging of a gastrin-releasing peptide receptor-positive tumor in a mouse model of human prostate cancer using a ^{64}Cu-labeled bombesin analogue. *Bioconjug Chem.* 2003;14:756–763.
28. Lamberts SW, Krenning EP, Reubi JC. The role of somatostatin and its analogs in the diagnosis and treatment of tumors. *Endocr Rev.* 1991;12:450–482.
29. Breeman WA, de Jong M, Kwekkeboom DJ, et al. Somatostatin receptor-mediated imaging and therapy: basic science, current knowledge, limitations and future perspectives. *Eur J Nucl Med.* 2001;28:1421–1429.
30. Virgolini I, Raderer M, Kurtaran A, et al. Vasoactive intestinal peptide-receptor imaging for the localization of intestinal adenocarcinomas and endocrine tumors. *N Engl J Med.* 1994;331:1116–1121.
31. Behr TM, Jenner N, Radetzky S, et al. Targeting of cholecystokinin-B/gastrin receptors in vivo: preclinical and initial clinical evaluation of the diagnostic and therapeutic potential of radiolabelled gastrin. *Eur J Nucl Med.* 1998;25:424–430.
32. Chen X, Park R, Shahinian AH, et al. ^{18}F-Labeled RGD peptide: initial evaluation for imaging brain tumor angiogenesis. *Nucl Med Biol.* 2004;31:179–189.
33. Haubner R, Wester HJ, Weber WA, et al. Noninvasive imaging of $\alpha_v\beta_3$ integrin expression using ^{18}F-labeled RGD-containing glycopeptide and positron emission tomography. *Cancer Res.* 2001;61:1781–1785.
34. Smith CJ, Volkert WA, Hoffman TJ. Gastrin releasing peptide (GRP) receptor targeted radiopharmaceuticals: a concise update. *Nucl Med Biol.* 2003;30:861–868.
35. Breeman WA, de Jong M, Erion JL, et al. Preclinical comparison of ^{111}In-labeled DTPA- or DOTA-bombesin analogs for receptor-targeted scintigraphy and radionuclide therapy. *J Nucl Med.* 2002;43:1650–1656.
36. Breeman WA, De Jong M, Bernard BF, et al. Pre-clinical evaluation of [^{111}In-DTPA-Pro^1,Tyr^4]bombesin, a new radioligand for bombesin-receptor scintigraphy. *Int J Cancer.* 1999;83:657–663.
37. Hoffman TJ, Gali H, Smith CJ, et al. Novel series of ^{111}In-labeled bombesin analogs as potential radiopharmaceuticals for specific targeting of gastrin-releasing peptide receptors expressed on human prostate cancer cells. *J Nucl Med.* 2003;44:823–831.
38. Smith CJ, Gali H, Sieckman GL, Higginbotham C, Volkert WA, Hoffman TJ. Radiochemical investigations of ^{99m}Tc-N_3S-X-BBN[7-14]NH_2: an in vitro/in vivo structure-activity relationship study where X = 0-, 3-, 5-, 8-, and 11-carbon tethering moieties. *Bioconjug Chem.* 2003;14:93–102.
39. Slice LW, Yee HF Jr, Walsh JH. Visualization of internalization and recycling of the gastrin releasing peptide receptor-green fluorescent protein chimera expressed in epithelial cells. *Recept Channels.* 1998;6:201–212.
40. Grady EF, Slice LW, Brant WO, Walsh JH, Payan DG, Bunnett NW. Direct observation of endocytosis of gastrin releasing peptide and its receptor. *J Biol Chem.* 1995;270:4603–4611.

JNM The Journal of NUCLEAR MEDICINE

microPET and Autoradiographic Imaging of GRP Receptor Expression with ^{64}Cu-DOTA-[Lys^{3}]Bombesin in Human Prostate Adenocarcinoma Xenografts

Xiaoyuan Chen, Ryan Park, Yingping Hou, Michel Tohme, Antranik H. Shahinian, James R. Bading and Peter S. Conti

J Nucl Med. 2004;45:1390-1397.

The Journal of Nuclear Medicine is published monthly.
SNMMI | Society of Nuclear Medicine and Molecular Imaging
1850 Samuel Morse Drive, Reston, VA 20190.
(Print ISSN: 0161-5505, Online ISSN: 2159-662X)

SNMMI SOCIETY OF NUCLEAR MEDICINE AND MOLECULAR IMAGING